Research Article
doi.org/10.1002/cbic.202200097

Chemistry Europe
European Chemical Societies Publishing

www.chembiochem.org

Structural Dynamics Support Electrostatic Interactions in the Active Site of Adenylate Kinase

Monsurat Motunrayo Lawal[a] and Valerie Vaissier Welborn*[a]

Electrostatic preorganization as well as structural and dynamic heterogeneity are often used to rationalize the remarkable catalytic efficiency of enzymes. However, they are often presented as incompatible because the generation of permanent electrostatic effects implies that the protein structure remains rigid. Here, we use a metric, electric fields, that can treat electrostatic contributions and dynamics effects on equal footing, for a unique perspective on enzymatic catalysis. We find that the residues that contribute the most to electrostatic interactions with the substrate in the active site of Adenylate Kinase (our working example) are also the most flexible residues. Further, entropy-tuning mutations raise flexibility at the picosecond timescale where more conformations can be visited on short time periods, thereby softening the sharp heterogeneity normally visible at the microsecond timescale.

Introduction

Electrostatic preorganization of protein scaffolds is responsible for the high enzymatic rate accelerations observed in nature.[1,2] Indeed, enzymatic scaffolds constitute an environment where short- and long-range electrostatic interactions facilitate substrate charge redistribution in the active site.[1–4] Compared to the same reaction in water, this results in the stabilization of the reaction transition state, which translates into an enthalpic reduction of the free activation energy ($\Delta G^{\ddagger}$):[5–7]

$$\Delta G^{\ddagger} = \Delta H^{\ddagger} - T\Delta S^{\ddagger}, \quad (1)$$

where $\Delta H^{\ddagger}$ and $\Delta S^{\ddagger}$ is the activation enthalpy and entropy, respectively. Within transition state theory,[8–10] this decrease in the free energy barrier yields improved reaction kinetics, where the reaction rate, k, is defined as:

$$k(T) = A(T)\exp\left(-\frac{\Delta G^{\ddagger}}{RT}\right). \quad (2)$$

Over the years, many have also considered entropic contributions to the reduction of $\Delta G^{\ddagger}$ in enzymes, although mostly through destabilization of the reactant state.[2,11,12] For example, desolvation effects[13–17] or higher ordering of the substrate in the active site[18–20] decrease the entropy of the reactant state, raising its free energy compared to the same reaction in water. However, these entropic effects were often shown to be negligible, leaving electrostatic enthalpics to rationalize enzymatic efficiency.[2,5,21,22]

The concept of electrostatic preorganization revolutionized the field of enzymatic catalysis because it attributed a functional role to protein scaffolds, in addition to their structural role. This means that, despite a very localized active site where only a few residues interact directly with the substrate (via hydrophobic interactions, covalent, hydrogen or ionic bonds), both scaffold and active site contribute to catalysis via electrostatic interactions. In this context, many have implied that rigid scaffolds were necessary to produce strong and permanent electrostatic interactions with the substrate in the active site.[23–26] In fact, the remarkable efficiency of the well-studied enzyme Ketosteroid Isomerase has been attributed to its stiff structure, which is thought to maximize electrostatic interactions from the scaffold with a minimally rearranging substrate.[27–31]

However, enzymes are also inherently dynamic structures. Indeed, protein motions such as thermal fluctuations, backbone and side chain rearrangements, local unfolding, etc. occur on disparate timescales, giving rise to characteristic "rugged" energy landscapes made of many conformational states of similar Boltzmann weights.[32–36] Many of these states are visited during the catalytic step, each exhibiting different catalytic proficiency, influencing the overall reaction kinetics.[37–39] However, the precise mechanism by which such structural dynamics influence catalysis has not been clearly identified, partly because the term "enzyme dynamics" has been used in the literature to describe widely different effects.[22] Some found that coupled motions throughout the protein accelerate the reaction by promoting the evolution of the reaction coordinate.[40–43] However, others have argued that these dynamical effects are short-ranged (less than 6 Å) and cannot include the scaffold.[5,44] Alternatively, others suggested that the evolutionary advantage of dynamical and conformational flexibility in proteins was to accommodate different reaction mechanisms in the active site,[45,46] which enables catalytic promiscuity and facilitate the evolution of new proteins and

[a] M. M. Lawal, V. Vaissier Welborn
Department of Chemistry, Virginia Tech Blacksburg, VA 24060 (USA)
E-mail: vwelborn@vt.edu

Supporting information for this article is available on the WWW under https://doi.org/10.1002/cbic.202200097

functions.[47–53] Finally, some refer to the process by which protein dynamics influence protein activity as dynamic allostery, in analogy with allosteric regulation of protein activity upon the binding of a drug or toxin.[54–56] Although all of these theories were verified convincingly for specific examples, they often focus on parts of the catalytic cycle other than the catalytic step (substrate binding, product release, catalytic promiscuity, etc.) and do not address the apparent discrepancy with the accepted electrostatic preorganization theory that imply a very precise (i.e. non-dynamic) positioning of catalytic residues.

In this paper, we present a computational study to simultaneously quantify the role of electrostatic interactions and structural dynamics on the catalytic step. For this purpose, we use a metric, electric fields ($\vec{E}$), that allows us to analyze electrostatic effects at molecular resolution.[3,57–59] With Vibrational Stark spectroscopy, Boxer and coworkers have previously demonstrated that the magnitude and orientation of electric fields in the active site of the enzyme Ketosteroid Isomerase correlate with its catalytic rate.[31,60] This can be rationalized by considering that the evolution of any chemical reaction can be determined by the breaking and formation of bonds, or the motion of electrons (charged particles), between atoms. This motion of electrons, which causes a change in bond dipole moments, will then be facilitated by an external electric field exerted along the reactive bonds (i.e., along the corresponding dipoles). Therefore, electric fields quantify the driving force ($\vec{F} = q\vec{E}$) behind the motion of electrons along specific bonds, which in turn quantifies how much the enzyme facilitates the reaction ($\Delta G^{\ddagger} \propto \vec{E}.\Delta\vec{\mu}$ where $\Delta\vec{\mu}$ is the change in bond dipole moment). The magnitude and orientation of electric fields are very sensitive to the geometry of the system, which makes them particularly well suited to analyze the effects of protein dynamics on $\vec{F}$, thereby the effects of protein dynamics on the catalytic step.

A paradigm of flexible protein is Adenylate Kinase (AdK), which catalyzes the reversible phosphoryl transfer reaction between adenosine triphosphate (ATP) and adenosine monophosphate (AMP):

$$\mathrm{ATP} + \mathrm{AMP} \leftrightarrow 2\mathrm{ADP}. \tag{3}$$

AdK consists of three structural domains, AMPb (residues 30–73), LID (122-159) and CORE (1-29, 74–121, 160–214). These domains undergo large scale conformational motions during the catalytic cycle where AdK transitions from an open, apo state to a closed bound state. Previous research focused on establishing a link between AdK dynamics and the interconversion between these two states,[32,52,56,61–63] without considering their direct influence on the evolution of the reaction (i.e., influence of protein structural dynamics in the closed state). Sequence analysis, single mutation experiments and simulations have identified a number of residues key to conformational transitions, such as Glu-10, Lys-13 and Arg-119.[61,64] Additionally, Arg-36, Arg-88 and Arg-119 were shown to be very dynamic residues whose side chains only exhibit good contact with the substrate in the closed state where they are more constricted.[61] This is consistent with the idea that the phosphate groups in AdK active site are stabilized by a network of highly conserved arginine residues: Arg-36, Arg-88, Arg-119, Arg-123, Arg-131 and Arg-167.[61,64–66] However, little is known about the role of residue dynamics on rate acceleration in the closed state and how it fits within the electrostatic preorganization theory.

Here, we present calculations of electric fields projected along the bond connecting the second to the third phosphate groups (i.e. the bond that would break during the reaction) in AdK bi-substrate transition state analog AP5 (PDB ID: 1AKE[67]). Note that the projection of the electric fields onto the active bond that best describe the evolution of the reaction results in electric field magnitudes that directly correlate to the enzyme's catalytic power. To identify the key residues that induce electrostatic interactions in the active site, we decompose the calculated electric fields into molecular contributions (k) that depend on space ($\vec{r}$) and time (t), as defined in Equation 1.

$$\begin{aligned}\vec{F}(\vec{r},t) &= q\vec{E}^{\text{total}}(\vec{r},t)\\ &= q\left(\vec{E}^{\text{water}}(\vec{r},t) + \vec{E}^{\text{residues}}(\vec{r},t) + \ldots\right)\\ &= q\sum_{k}\vec{E}^{k}(\vec{r},t)\end{aligned} \tag{4}$$

We assess electrostatic preorganization and structural dynamics effects by comparing the wild type (WT) to four AdK mutants engineered with entropy tuning mutations (to Gly) at distal sites.[68] Mutation to glycine at surface exposed sites were shown to be frequent in enzymes operating at cold temperatures, suggesting that dynamic allostery controls protein

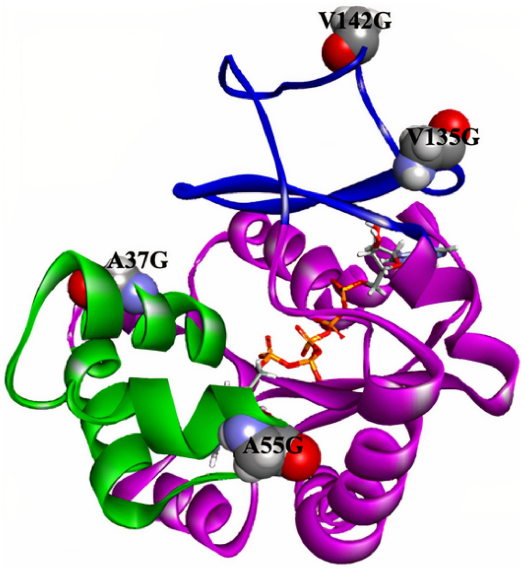

Figure 1. Structure of *E. coli* Adenylate Kinase (AdK) complexed with bi-substrate analog AP5 (PDB code: 1AKE[67]). The four mutation sites investigated here are shown: Ala37Gly and Ala55Gly in AMPb domain; Val135Gly and Val142Gly in LID domain. CORE (in pink) consists of residues 1–29, 74–121 and 160–214; AMPb (in green) consists of residues 30–73; and LID (in blue) consists of residues 122–159.

adaptation to the environment.[50,68] In the context of AdK, the mutants Ala37Gly, Ala55Gly, Val135Gly and Val142Gly (Figure 1) were shown experimentally to yield higher affinity or turnover than AdK WT, primarily due to changes in the flexibility of LID and AMPb structural domains.[63,68] In this computational study, we focus on the catalytic step (closed state) to link short timescale structural dynamics (short compared to the timescale on which occur the large conformational motions that drive the interconversion between states) fits within the electrostatic preorganization theory.

The MD trajectories and electric field data will be made available on our group's Github upon publication (https://github.com/WelbornGroup).

Computational Methods

System preparation: The starting AdK structure is available in the protein data bank with code, 1AKE[67] co-crystallized with AP5 and refined at 1.9 Å resolution. We use the REDUCE program[69] to add hydrogen to the structure while the Gly mutations were introduced with MODELLER, generating five different AdK-AP5 complexes of WT, Ala37Gly, Ala55Gly, Val135Gly, and Val142Gly.

Conformation sampling: The two steps involved in creating the 25 different structures for each system are backbone conformational search and side-chain ensemble simulation. We use the backrub algorithm[70,71] from the ROSETTA package to generate 25 uncorrelated low energy backbone conformations from $25 \times 10,000$ trials. The backrub algorithm rotates the protein backbone as a static body about the alpha carbon, C_α.[71] We then repacked the side chains for the 25 low energy backbone structures, using the fixbb algorithm from ROSETTA. Fixbb is a Monte Carlo method that samples the Dunbrack backbone-dependent rotamer library.

MD simulations: We use PACKMOL[72] to determine the periodic boundary conditions for each protein, with a 10 Å buffer on either side. We then used Gromacs[73] to solvate and neutralize the system. Each mutant was then minimized with steepest descent, using the AMOEBA[74] polarizable force field. Parameters for the inhibitor AP5 were added following the protocol in Reference. Equilibration was performed in the NVT ensemble for 150 ps (1 fs timestep), which was followed by 150 ps production run (1 fs timestep) in the NPT ensemble. Nose-Hoover thermostat and barostat were used in combination with the Beeman velocity integrator and particle mesh Ewald algorithm for long-range electrostatics. Data showing the convergence of the MD after equilibration is available in Supporting Information.

Post MD analyses: We used the CPPTRAJ module[75] to calculate the RMSD, RMSF and RoG.

$$\mathrm{RMSD}(v,w) = \sqrt{1/n \sum_{i=1}^{n} (v_i - w_i)^2}, \tag{5}$$

where v_i and w_i are the coordinates of Cα atom in v and w at the time i, respectively.

$$\mathrm{RMSF} = \sqrt{1/n \sum_{n}^{j} (x_{i(j)} - x_i)^2}, \tag{6}$$

where $x_{i(j)}$ represents the position of the i-th atom in the coordinate of the j-th model, and (x_i) denotes the average position of the i-th atoms in all models.

$$\mathrm{RoG} = \sqrt{1/n \sum_{n}^{i=0} (r_i - r_m)^2}, \tag{7}$$

where r_i denotes atomic position and r_m denotes the mean position of all atoms.

The electric fields were calculated every 1 ps of the 150 ps NPT production run, for each mutant. The fields were computed with ELECTRIC[76] and projected onto the bond connecting the second to the third phosphate groups in the AP5 inhibitor. The MD trajectories and electric field data will be made available on our group's Github upon publication (https://github.com/WelbornGroup).

Results

We sample protein motions by running 150 ps NPT production molecular dynamics (MD) simulations on 25 independent protein structures for each AdK mutants (Ala37Gly, Ala55Gly, Val135Gly and Val142Gly) and WT. The 25 structures are obtained by sampling low-energy backbone and side chain conformations with the Rosetta package algorithms (see Methods). This provides us with short-time dynamics that sample thermal fluctuations, solvent relaxation and molecular motions (ps timescale) over an ensemble that characterizes backbone and side chain rearrangements (μs timescale). Enzyme properties can then be estimated by quantity averages over both the MD trajectories and the conformational ensemble. To structural dynamics to electrostatic preorganization, we want to capture the protein dynamics in the closed (bound) state of AdK, for all mutants. In Figures 2–3, we present the average root-mean-square-deviation (RMSD) and radius of gyration (RoG) of LID, the structural domain that controls binding. We see that the average structure of the WT and all mutants is identical, as we would expect for single mutations at surface sites, confirming that our data characterizes the same closed conformational state. For completeness, we provide in Supporting Information the average Root-Mean-Square-Fluctuation (RMSF) and RoG of the AMPb and CORE domains.

Using this data, we calculate the electric fields projected onto the bond connecting the second to the third phosphate groups in the AP5 inhibitor. The electric fields were computed using our in-house code ELECTRIC,[76] as a post-processing step on the MD trajectories, performed with the AMOEBA polarizable force field[74,77,78] (see Methods). The projected electric fields, averaged over the MD trajectories and the conformational ensemble are presented in Figure 4.

We observe significant contributions from residues from all three domains (CORE, LID and AMPb), an indication that the CORE domain does not solely contributes to the catalytic step. In other words, Figure 4 shows that Adk is preorganized such that residues across these domains have strong electrostatic interactions with the substrate in the active site. Further, we see

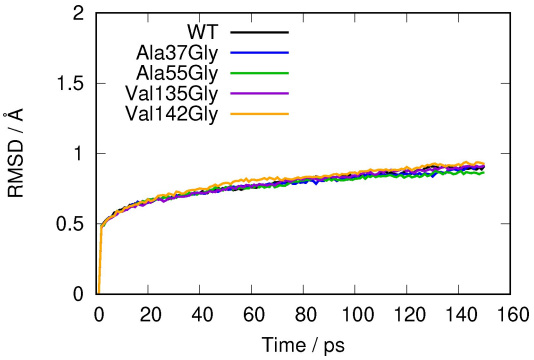

Figure 2. Average Root-Mean-Square-Deviation (RMSD) of AdK WT and mutants. The LID domain has been shown, experimentally and theoretically, to undergo large-scale motions, even yielding local unfolding, when Adk transitions from closed to open state.[63,68] Here, we focus on the close state where each structural domain only undergoes small length-scale motions.

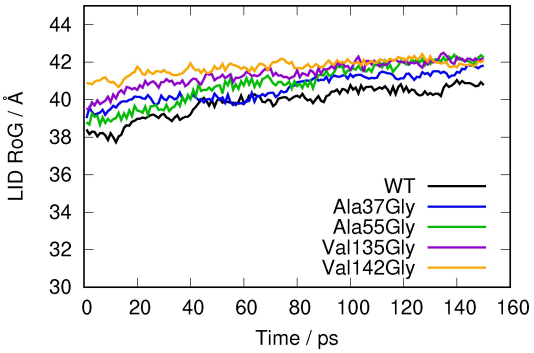

Figure 3. Average LID Radius of Gyration (RoG). The LID domain has been shown, experimentally and theoretically, to undergo large-scale motions, even yielding local unfolding, when Adk transitions from closed to open state.[63,68] Here, we focus on the close state where each structural domain only undergoes small length-scale motions.

that the average electric fields for each mutant is very similar to the average electric fields of the WT, with only a visible difference for residues Lys-13 and Arg-167. This is consistent with our structural data showing that all mutants have the same average structure. This means that the entropy-tuning mutations, experimentally proven to yield to a change in catalytic activity,[68] do not have a visible effect on the averaged protein properties. This would suggest that changes in catalytic rates come from fluctuations around this average; a dynamical effect. To verify this hypothesis, we calculate the electric field fluctuations, separating the ps timescale (fluctuations over time during the MD simulations) and the μs timescale (fluctuations over the conformational ensemble). In Figure 5, we present the standard deviation for the AdK WT and all mutants at the ps timescale (σ^{ps}) while in Figure 6, we present the standard deviation at the μs timescale ($\sigma^{\mu s}$).

In Figures 5 and 6, we note that the residues exhibiting the highest fluctuations overlap significantly with the residues exhibiting the strongest projected electric fields (Figure 4). This suggests a coupling between electrostatic preorganization of the protein structure and structural dynamics, whereby the

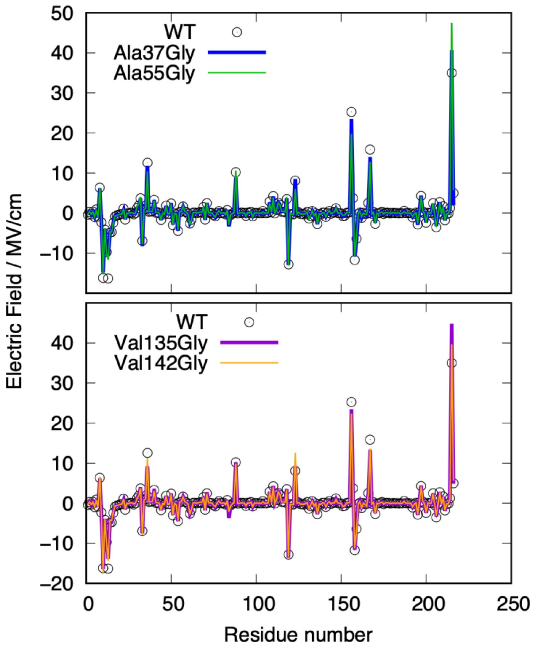

Figure 4. Average electric fields projected onto the bond connecting the second to the third phosphate groups in the AP5 inhibitor. Top: the two AMPb mutants, Ala37Gly and Ala55Gly, compared to wild type. Bottom: the two LID mutants, Val135Gly and Val142Gly, compared to WT. The fields are given in MV/cm as a function of residue number. Residues 1–214 are the AdK protein, residue 215 is the water and residue 216 the counter ions maintaining overall charge neutrality.

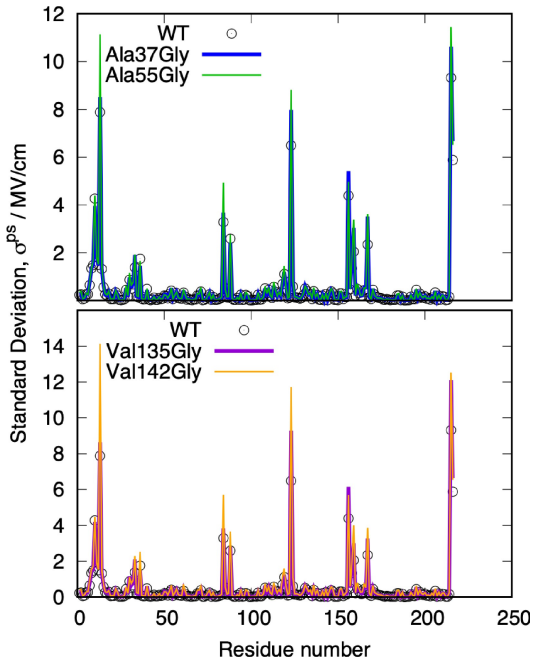

Figure 5. Picosecond timescale standard deviation of the projected electric fields. The standard deviation was calculated using the data of the 150 ps NPT trajectories. Top: the two AMPb mutants, Ala37Gly and Ala55Gly, compared to wild type. Bottom: the two LID mutants, Val135Gly and Val142Gly, compared to WT. The standard deviation is given in MV/cm as a function of residue number. Residues 1–214 are the AdK protein, residue 215 is the water and residue 216 the counter ions maintaining overall charge neutrality.

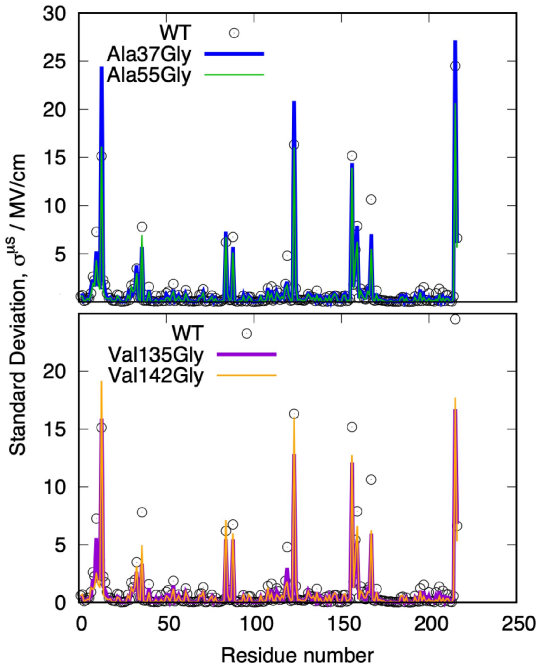

Figure 6. Microsecond timescale standard deviation of the projected electric fields. The standard deviation was calculated using the data of the conformational ensemble characterizing backbone and side chain protein motions. Top: the two AMPb mutants, Ala37Gly and Ala55Gly, compared to wild type. Bottom: the two LID mutants, Val135Gly and Val142Gly, compared to WT. The standard deviation is given in MV/cm as a function of residue number. Residues 1–214 are the AdK protein, residue 215 is the water and residue 216 the counter ions maintaining overall charge neutrality.

residues interacting with the substrate in the active site are also the most flexible residues in the closed state. We also observe significant differences in the magnitude of σ, both at the ps and μs timescale between the mutants and the WT. Overall, there is an increase in the fluctuations for most residues at the picosecond timescale and an attenuation of the fluctuations at the microsecond timescale, compared to WT. This means that the entropy-tuning mutations allow for more flexibility at the picosecond timescale, accommodating more side chain conformations, which softens the differences between conformations at the microsecond timescale. A notable exception comes from Lys-13, exhibiting enhanced fluctuations at the ps and the μs timescale. Structural analysis of the ensembles confirmed that the μ fluctuations in projected electric fields come from different rotamers of individual residues visited during the simulations (see Supporting Information for Lys-13 and Arg-167).

Finally, in Table 1, we summarize the data presented in Figures 4–6 by looking at average projected electric fields and fluctuations over the three structural domains of AdK.

We see that the CORE and LID domains are significantly more flexible than the AMPb domain. Previous studies emphasized the flexibility of the LID domain, although not at these time scales, and the rigidity of the AMPb domain locked in place after binding the substrate.[63,68,79] Here, we can see that domain flexibility is also visible on the picosecond timescale

Table 1. Average projected electric fields, standard deviation over ps and μs for AdK WT and the four entropy-inducing mutants, per structural domain. AMPb (residues 30–73), LID (122-159) and CORE (1-29, 74–121, 160–214).

Mutant	CORE $\langle \vec{E}.\vec{u} \rangle$	σ^{ps}	$\sigma^{\mu s}$	AMPb $\langle \vec{E}.\vec{u} \rangle$	σ^{ps}	$\sigma^{\mu s}$	LID $\langle \vec{E}.\vec{u} \rangle$	σ^{ps}	$\sigma^{\mu s}$
WT	−31.5	11.1	24.1	14.5	2.8	9.8	12.9	8.3	24.5
Ala37Gly	−24.0	11.8	28.6	12.8	3.0	7.7	11.1	10.4	27.1
Ala55Gly	−31.6	14.6	20.5	12.9	3.3	8.3	6.1	11.0	22.7
Val135Gly	−25.9	12.1	20.7	12.0	3.3	5.5	13.9	11.8	19.1
Val142Gly	−26.2	17.6	23.1	12.1	4.2	6.7	14.0	13.9	22.1

and that the CORE domain is as flexible as the LID domain. Since many residues involved in the catalytic step are located in CORE, the observed flexibility of CORE couples structural dynamics to electrostatic preorganization in AdK. We also observe that the effects of the mutations are delocalized throughout the protein structure with the AMPb mutations (Ala37Gly and Ala55Gly) causing enhanced flexibility of the LID and CORE domains, just as the LID mutations (Val135Gly and Val142Gly).

Discussion

In this paper, we presented a series of molecular dynamics simulations of AdK WT and four AdK Gly mutants designed to enhance entropy effects. We characterized various conformational ensemble using electric fields to establish a direct link between dynamic and functional effects within the electrostatic preorganization theory. We found that the protein residues that contribute the most to the orientation and magnitude of the electric fields yielding bond breaking and formation in the active site are also the most flexible residues. This provides a new interpretation of electrostatic preorganization whereby protein scaffolds do not need to be stiff structures to induce strong and permanent electrostatic effects in the active site. This also reconciles electrostatic catalysis with structural dynamics, two properties that are often considered incompatible and treated independently, despite being highly conserved through evolution. We note that this is also consistent with a recent study by Kumawat et al. that attributed dynamic allosteric effects to electrostatic interactions in PDZ domains.[55]

Finally, we note that the use of electric fields allows for a unified analysis of the key contributors to catalysis. Figure 7 shows the main contributors to electric field magnitude and fluctuations, identified in this study without requiring prior knowledge of the mechanism of AdK. Many of the residues listed here were identified across multiple independent experimental or theoretical studies. Some were only identified after single mutation experiments specifically seeking out the contribution of residues conserved through evolution and AdK forms, as for the dynamic network of arginine residues stabilizing the substrate in the active site.[66] In Figure 7, five out of the eight highlighted residues are arginines, naturally bringing forward the key role these residues play in the catalytic step. Additionally, we note that the electric field metric allows

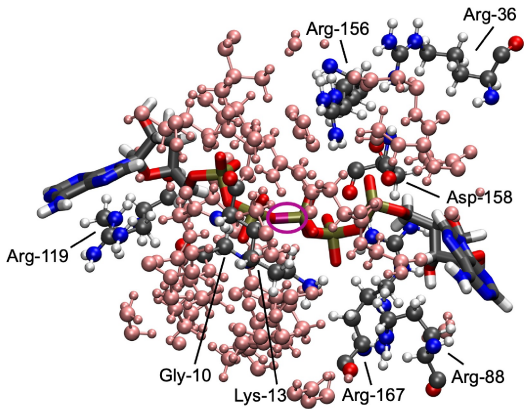

Figure 7. Top contributors to the electric field magnitude and fluctuations identified in this study. For comparison, we show in pink the residues that would be included with a purely structural study, including all residues within 5 Å of the bond of interest.

for a more targeted approach than what structural information could offer as is shown comparing our list of top contributors to the list of residues within 5 Å of the bond of interest (in pink in Figure 7).

The coupled role of electrostatic preorganization and structural dynamics is key to advance our understanding our enzymatic catalysis, which can, in turn, assist in the rational design of drugs to regulate protein activity or the engineering of synthetic enzymes.

Acknowledgements

The authors thank the Virginia Tech Department Faculty Start-up Funds for financial support and acknowledge Advanced Research Computing at Virginia Tech (https://arc.vt.edu) for providing computational resources and technical support that have contributed to the results reported within this paper.

Conflict of Interest

The authors declare no conflict of interest.

Data Availability Statement

Data will be made available on the PI's group Github upon publication.

Keywords: molecular dynamics · structural dynamics · polarizable force field · electric field · electrostatic preorganizationadenylate kinase

[1] A. Warshel, P. K. Sharma, M. Kato, Y. Xiang, H. Liu, M. H. Olsson, *Chem. Rev.* **2006**, *106*, 3210–3235.
[2] A. Warshel, *J. Biol. Chem.* **1998**, *273*, 27035–27038.
[3] M. R. Hennefarth, A. N. Alexandrova, *Curr. Opin. Struct. Biol.* **2022**, *72*, 1–8.
[4] A. Morgenstern, M. Jaszai, M. E. Eberhart, A. N. Alexandrova, *Chem. Sci.* **2017**, *8*, 5010–5018.
[5] V. Vaissier Welborn, T. Head-Gordon, *Chem. Rev.* **2019**, *119*, 6613–6630.
[6] D. Burschowsky, A. van Eerde, M. Ökvist, A. Kienhöfer, P. Kast, D. Hilvert, U. Krengel, *Proc. Nat. Acad. Sci.* **2014**, *111*, 17516–17521.
[7] S. Martí, J. Andrés, V. Moliner, E. Silla, I. Tuñón, J. Bertrán, *J. Am. Chem. Soc.* **2004**, *126*, 311–319.
[8] V. L. Schramm, *J. Biol. Chem.* **2007**, *282*, 28297–28300.
[9] M. H. Olsson, J. Mavri, A. Warshel, *Philos. Trans. R. Soc. Lond., B, Biol. Sci.* **2006**, *361*, 1417–1432.
[10] K. Zinovjev, I. Tuñón, *Proc. Nat. Acad. Sci.* **2017**, *114*, 12390–12395.
[11] M. Kazemi, F. Himo, J. Åqvist, *Proc. Nat. Acad. Sci.* **2016**, *113*, 2406–2411.
[12] L. D. Andrews, T. D. Fenn, D. Herschlag, *PLoS Biol.* **2013**, *11*, e1001599.
[13] J. K. Lee, K. Houk, *Science* **1997**, *276*, 942–945.
[14] A. P. Borole, C. L. Cheng, B. H. Davison, *Biotechnol. Prog.* **2004**, *20*, 1251–1254.
[15] E. Araújo, A. H. Lima, J. Lameira, *Phys. Chem. Chem. Phys.* **2017**, *19*, 21350–21356.
[16] J. P. Richard, T. L. Amyes, B. Goryanova, X. Zhai, *Curr. Opin. Struct. Biol.* **2014**, *21*, 1–10.
[17] P.-O. Syrén, S. C. Hammer, B. Claasen, B. Hauer, *Angew. Chem.* **2014**, *126*, 4945–4949; *Angew. Chem. Int. Ed.* **2014**, *53*, 4845–4849.
[18] D. N. Poshina, S. V. Raik, A. A. Sukhova, I. V. Tyshkunova, D. P. Romanov, E. V. Eneyskaya, A. A. Kulminskaya, Y. A. Skorik, *Carbohydr. Res.* **2020**, *498*, 108191.
[19] H. Fromm, *Eur. J. Biochem.* **1969**, *7*, 385–392.
[20] J. M. Fox, K. Kang, M. Sastry, W. Sherman, B. Sankaran, P. H. Zwart, G. M. Whitesides, *Angew. Chem.* **2017**, *129*, 3891–3895; *Angew. Chem. Int. Ed.* **2017**, *56*, 3833–3837.
[21] J. Lameira, R. P. Bora, Z. T. Chu, A. Warshel, *Proteins* **2015**, *83*, 318–330.
[22] S. C. Kamerlin, A. Warshel, *Proteins Struct. Funct. Bioinf.* **2010**, *78*, 1339–1375.
[23] K. Swiderek, I. Tunon, V. Moliner, J. Bertran, *ACS Catal.* **2015**, *5*, 2587–2595.
[24] A. J. Adamczyk, J. Cao, S. C. Kamerlin, A. Warshel, *Proc. Nat. Acad. Sci.* **2011**, *108*, 14115–14120.
[25] N. Preiswerk, T. Beck, J. D. Schulz, P. Milovník, C. Mayer, J. B. Siegel, D. Baker, D. Hilvert, *Proc. Nat. Acad. Sci.* **2014**, *111*, 8013–8018.
[26] W. J. Song, J. Yu, F. A. Tezcan, *J. Am. Chem. Soc.* **2017**, *139*, 16772–16779.
[27] S. C. Kamerlin, P. K. Sharma, Z. T. Chu, A. Warshel, *Proc. Nat. Acad. Sci.* **2010**, *107*, 4075–4080.
[28] M. R. Hennefarth, A. N. Alexandrova, *ACS Catal.* **2020**, *10*, 9915–9924.
[29] Y. Wu, S. D. Fried, S. G. Boxer, *J. Am. Chem. Soc.* **2020**, *142*, 9993–9998.
[30] L. Wang, S. D. Fried, T. E. Markland, *J. Phys. Chem. B* **2017**, *121*, 9807–9815.
[31] S. D. Fried, S. Bagchi, S. G. Boxer, *Science* **2014**, *346*, 1510–1514.
[32] D. Li, M. S. Liu, B. Ji, *Biophys. J.* **2015**, *109*, 647–660.
[33] S. J. Benkovic, G. G. Hammes, S. Hammes-Schiffer, *Biochem.* **2008**, *47*, 3317–3321.
[34] D. D. Boehr, D. McElheny, H. J. Dyson, P. E. Wright, *Science* **2006**, *313*, 1638–1642.
[35] N. G. Leferink, S. Hay, S. E. Rigby, N. S. Scrutton, *FEBS J.* **2015**, *282*, 3016–3029.
[36] T. D. Romo, A. Grossfield, A. G. Markelz, *J. Chem. Inf. Model.* **2020**, *60*, 6419–6426.
[37] R. García-Meseguer, S. Martí, J. J. Ruiz-Pernía, V. Moliner, I. Tuñón, *Nat. Chem.* **2013**, *5*, 566–571.
[38] K. Swiderek, I. Tuñón, V. Moliner, J. Bertrán, *Chem. Eur. J.* **2017**, *23*, 7582–7589.
[39] M. A. Maria-Solano, E. Serrano-Hervás, A. Romero-Rivera, J. Iglesias-Fernández, S. Osuna, *Chem. Commun.* **2018**, *54*, 6622–6634.
[40] P. K. Agarwal, S. R. Billeter, P. R. Rajagopalan, S. J. Benkovic, S. Hammes-Schiffer, *Proc. Nat. Acad. Sci.* **2002**, *99*, 2794–2799.
[41] D. Antoniou, S. D. Schwartz, *J. Phys. Chem. B.* **2011**, *115*, 15147–15158.
[42] A. Kohen, *Acc. Chem. Res.* **2015**, *48*, 466–473.
[43] G. Bhabha, J. T. Biel, J. S. Fraser, *Acc. Chem. Res.* **2015**, *48*, 423–430.
[44] N. Boekelheide, R. Salomón-Ferrer, T. F. Miller, *Proc. Nat. Acad. Sci.* **2011**, *108*, 16159–16163.
[45] X. Pan, S. D. Schwartz, *J. Phys. Chem. B* **2015**, *119*, 5430–5436.
[46] X. Chen, S. D. Schwartz, *Biochem.* **2018**, *57*, 3289–3298.
[47] N. Tokuriki, D. S. Tawfik, *Curr. Opin. Struct. Biol.* **2009**, *19*, 596–604.

[48] N. Tokuriki, D. S. Tawfik, *Science* **2009**, *324*, 203–207.
[49] L. C. James, D. S. Tawfik, *Trends Biochem. Sci.* **2003**, *28*, 361–368.
[50] H. Mohamadnezhadi, A. Beiramzadeh, M. Shadman Lakmehsari, K. Khalifeh, E. Heshmati, *J. Biomol. Struct. Dyn.* **2019**, *37*, 2110–2117.
[51] P. K. Agarwal, D. N. Bernard, K. Bafna, N. Doucet, *ChemCatChem* **2020**, *12*, 4704–4720.
[52] L. G. Ahuja, A. P. Kornev, C. L. McClendon, G. Veglia, S. S. Taylor, *Proc. Nat. Acad. Sci.* **2017**, *114*, E931–E940.
[53] M. J. Varga, M. W. Dzierlenga, S. D. Schwartz, *Biochem.* **2017**, *56*, 2488–2496.
[54] G. R. Bowman, P. L. Geissler, *Proc. Nat. Acad. Sci.* **2012**, *109*, 11681–11686.
[55] A. Kumawat, S. Chakrabarty, *Proc. Nat. Acad. Sci.* **2017**, *114*, E5825–E5834.
[56] L. G. Ahuja, P. C. Aoto, A. P. Kornev, G. Veglia, S. S. Taylor, *Proc. Nat. Acad. Sci.* **2019**, *116*, 15052–15061.
[57] V. V. Welborn, T. Head-Gordon, *J. Am. Chem. Soc.* **2019**, *141*, 12487–12492.
[58] V. V. Welborn, L. R. Pestana, T. Head-Gordon, *Nat. Catal.* **2018**, *1*, 649–655.
[59] V. Vaissier, S. C. Sharma, K. Schaettle, T. Zhang, T. Head-Gordon, *ACS Catal.* **2018**, *8*, 219–227.
[60] E. S. Park, S. S. Andrews, R. B. Hu, S. G. Boxer, *J. Phys. Chem. B* **1999**, *103*, 9813–9817.
[61] E. Formoso, V. Limongelli, M. Parrinello, *Sci. Rep.* **2015**, *5*, 8425.
[62] Y. Wang, L. Makowski, *Proteins* **2018**, *86*, 332–343.
[63] H. Song, Y. Wutthinitikornkit, X. Zhou, J. Li, *J. Chem. Phys.* **2021**, *155*, 035101.
[64] H. Krishnamurthy, H. Lou, A. Kimple, C. Vieille, R. I. Cukier, *Proteins* **2005**, *58*, 88–100.
[65] T. Ogura, S. W. Whiteheart, A. J. Wilkinson, *J. Struct. Biol.* **2004**, *146*, 106–112.
[66] T. Dahnke, Z. Shi, H. Yan, R. T. Jiang, M. D. Tsai, *Biochem.* **1992**, *31*, 6318–6328.
[67] C. W. Müller, G. E. Schulz, *J. Mol. Biol.* **1992**, *224*, 159–177.
[68] H. G. Saavedra, J. O. Wrabl, J. A. Anderson, J. Li, V. J. Hilser, *Nature* **2018**, *558*, 324–328.
[69] J. M. Word, S. C. Lovell, J. S. Richardson, D. C. Richardson, *J. Mol. Biol.* **1999**, *285*, 1735–1747.
[70] I. W. Davis, W. B. Arendall III, D. C. Richardson, J. S. Richardson, *Structure* **2006**, *14*, 265–274.
[71] C. A. Smith, T. Kortemme, *J. Mol. Biol.* **2008**, *380*, 742–756.
[72] L. Martínez, R. Andrade, E. G. Birgin, J. M. Martínez, *J. Comput. Chem.* **2009**, *30*, 2157–2164.
[73] D. Van Der Spoel, E. Lindahl, B. Hess, G. Groenhof, A. E. Mark, H. J. Berendsen, *J. Comput. Chem.* **2005**, *26*, 1701–1718.
[74] C. Zhang, C. Lu, Z. Jing, C. Wu, J.-P. Piquemal, J. W. Ponder, P. Ren, *J. Chem. Theory Comput.* **2018**, *14*, 2084–2108.
[75] D. R. Roe, T. E. Cheatham III, *J. Chem. Theory Comput.* **2013**, *9*, 3084–3095.
[76] J. Nash, T. Barnes, V. V. Welborn, *J. Open Source Softw.* **2020**, *5*, 2576.
[77] Y. Shi, Z. Xia, J. Zhang, R. Best, C. Wu, J. W. Ponder, P. Ren, *J. Chem. Theory Comput.* **2013**, *9*, 4046–4063.
[78] J. W. Ponder, C. Wu, P. Ren, V. S. Pande, J. D. Chodera, M. J. Schnieders, I. Haque, D. L. Mobley, D. S. Lambrecht, R. A. DiStasio Jr, *J. Phys. Chem. B* **2010**, *114*, 2549–2564.
[79] F. Zeller, M. Zacharias, *Biophys. J.* **2015**, *109*, 1978–1985.

Manuscript received: February 16, 2022
Revised manuscript received: March 17, 2022
Accepted manuscript online: March 18, 2022
Version of record online: April 1, 2022